# High-precision (p,t) reactions to determine reaction rates of explosive stellar processes

Matić, Andrija

# Chapter 6

# $^{26}$Si data and their astrophysical implications

In this chapter we will discuss in detail the $^{28}$Si(p,t)$^{26}$Si data. Our data will be compared with previous results and possible spin assignments will be given. All data will be included in the $^{25}$Al(p,$\gamma$)$^{26}$Si and $^{22}$Mg($\alpha$,p)$^{25}$Al reaction-rate calculations.

The angular distributions for the g.s. $0^+$, 1.796 MeV $2^+$ and 5.512 MeV $4^+$ levels obtained in the $^{28}$Si(p,t)$^{26}$Si reaction are presented in Fig. 6.1 together with the angular distributions calculated with DWUCK4. A description of the input parameters for the DWBA calculations can be found in Appendix A. In this case also, we found a discrepancy between the measured and calculated angular distributions similar to that found for the $^{24}$Mg(p,t)$^{22}$Mg reaction. Therefore, for $^{26}$Si levels which have unknown spin-parity values, we will rely on the mirror spin-parity assignments using information for mirror levels in $^{26}$Mg.

## 6.1 $^{26}$Si and its mirror nucleus $^{26}$Mg

$^{26}$Si is an unstable, proton-rich nucleus with a half-life of 2.23 s. In the present $^{28}$Si(p,t)$^{26}$Si experiment we obtained high-resolution $^{26}$Si spectra (see next three sections). Similar to the discussion on $^{22}$Mg presented in Chapter 5 we need additional data to perform reaction-rate calculations. We were not able to obtain spin-parity information for the $^{26}$Si levels directly from our experiment and there are no resonance-strength data for the $^{25}$Al(p,$\gamma$)$^{26}$Si or $^{22}$Mg($\alpha$,p)$^{25}$Al reactions. Consequently, we used the mirror nucleus of $^{26}$Si, which is $^{26}$Mg, as a source for missing information that is necessary to perform the calculations for the $^{25}$Al(p,$\gamma$)$^{26}$Si and $^{22}$Mg($\alpha$,p)$^{25}$Al reactions.

$^{26}$Mg is a stable nucleus with a natural isotopic abundance of 11.01%. Consequently, its nuclear structure is much better known than that of $^{26}$Si. Information on levels (i.e. excitation energy and spin-parity) in $^{26}$Mg can be found in Ref. [61]. Using proton, neutron, $^{25}$Al, and $^{25}$Si nuclear masses from Ref. [53] and $^{22}$Mg and $^{26}$Si masses from Ref. [49], we calculated the proton, alpha, and neutron-emission thresholds in $^{26}$Mg to be 14.1458 MeV, 10.6148 MeV, and 11.0931 MeV, respectively.

Since $\Gamma_\gamma$ values for levels in $^{26}$Si are needed to calculate the $^{25}$Al(p,$\gamma$)$^{26}$Si reaction rates (see Section 6.5), we determined them by comparing to mirror levels in $^{26}$Mg, because all $^{26}$Mg levels below the $\alpha$-emission threshold can decay only via $\gamma$-decay. The spin-parity values for levels in $^{26}$Mg are known up to 9.2 MeV with a few exceptions. Therefore, these values are used to assign the spin-parity values for levels in $^{26}$Si.

The $\Gamma_p$ values are calculated using $^{26}$Mg single-particle (neutron) spectroscopic factors from Ref. [69], which have been corrected with single-particle reduced widths taken from Ref. [70], see Section 6.5.

The $S_\alpha$ values for $^{26}$Si, necessary for the $^{22}$Mg($\alpha$,p)$^{25}$Al reaction-rate calculations, are taken from its mirror nucleus, $^{26}$Mg, see Section 6.6. These values are calculated from the data of Ref. [71].

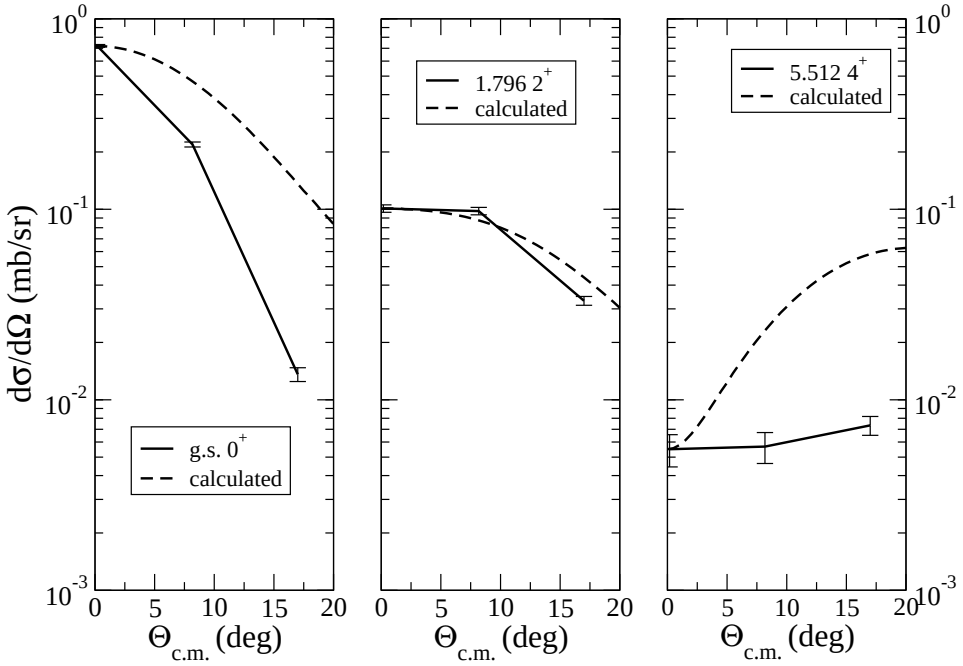


**Figure 6.1**: *The measured and calculated angular distributions for the g.s. $0^+$, 1.796 MeV $2^+$ and 5.512 MeV $4^+$ levels of $^{26}$Si. See further Fig. 4.5 for more details. The solid line is used to guide the eye.*

## 6.2 Calibration region (g.s. - 5.5123 MeV)

In this section we will discuss levels below the proton-emission threshold. In Fig 4.10, spectra obtained at spectrometer angles $-0.3°$, $8°$ and $17°$ are shown with calibration levels indicated with a $^*$. In Fig 6.2, we display a blow-up of the same $^{26}$Si spectra for the excitation-energy region from 4 to 5.6 MeV.

The deduced energies of excited states in $^{26}$Si below the proton-emission threshold are listed in the third column of Table 6.1; previous experimental results are listed in columns 4 to 10. The adopted spin-parity values for the $^{26}$Si nucleus, taken from Ref. [29] are listed in the first column of Table 6.1 and the mirror assigned spin-parity values are listed in the second column.

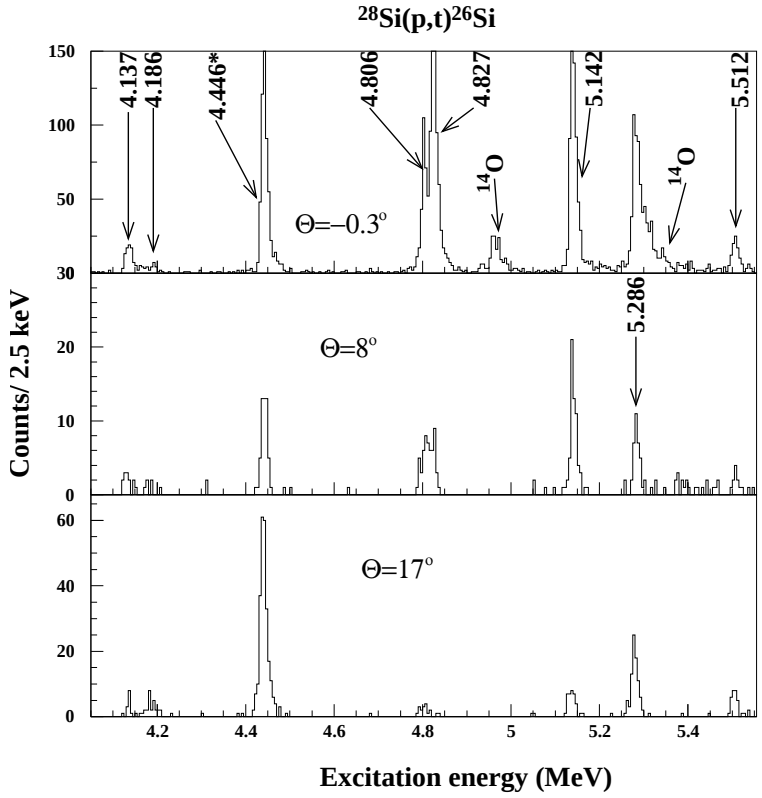


**Figure 6.2**: *$^{26}$Si spectra in the region 4 to 5.6 MeV taken at spectrometer angles $-0.3°$, $8°$, and $17°$. A resolved doublet at 4.806 MeV and 4.827 MeV can be observed. The calibration line is marked with $^*$. The determined excitation energies for $^{26}$Si are listed in the third column of Table 6.1. See further Fig. 4.5 for more details.*

**Table 6.1**: *The calibration region encompassing the $^{26}$Si excitation energies below the proton-emission threshold, i.e. 5.5123 MeV, with the adopted spin-parity assignments.*

| $J^\pi$ adopted[b] | $J^\pi$ mirror[c] | Present (p,t) | Ref. [29] ($^3$He,n) | Ref. [28] ($^3$He,$^6$He) | Ref. [27] (p,t) | Ref. [72] ($^3$He,n) | Ref. [73] (p,t) | Ref. [74] ($^3$He,n) | Ref. [46] compilation | adopted present[d] |
|---|---|---|---|---|---|---|---|---|---|---|
| $0^+$ | $0^+$ | g.s.* | g.s.[a] | g.s.[a] | g.s.[a] | g.s. | g.s. | g.s. | g.s. | g.s. |
| $2^+$ | $2^+$ | 1.7959* | 1.7959[a] | 1.7959[a] | 1.7959[a] | 1.800(30) | 1.795(11) | 1.7959(2) | 1.7959(2) | 1.7959(2) |
| $2^+$ | $2^+$ | 2.7835* | 2.7835[a] | 2.7835[a] | 2.7835[a] | 2.780(30) | 2.790(12) | 2.7835(4) | 2.7835(4) | 2.7835(4) |
| $0^+$ | $0^+$ | 3.3325* | 3.3325[a] | - | 3.3325[a] | 3.330(30) | 3.339(19) | 3.3325(3) | 3.3325(3) | 3.3325(3) |
| - | $(3^+)$ | (3.749(4)) | 3.756[a] | - | 3.756[a] | 3.760(30) | - | 3.756(2) | 3.756(2) | 3.756(2) |
| - | - | - | - | - | - | - | - | 3.842(2) | 3.842(2) | 3.842(2) |
| - | $(4^+)$ | - | - | - | - | - | - | (4.093(3)) | (4.093(3)) | (4.093(3)) |
| $2^+$ | $2^+$ | 4.1366(28) | 4.138(4) | 4.144(8) | 4.155(2) | 4.140(30) | - | 4.138(1) | 4.138(1) | 4.1379(9) |
| $3^+$ | $3^+$ | 4.186(4) | 4.183(4) | 4.211(16) | 4.155(2) | - | 4.183(11) | - | 4.183(11) | 4.1854(27) |
| $2^+$ | $2^+$ | 4.446* | 4.446[a] | 4.446[a] | 4.445[a] | 4.450(30) | 4.457(13) | 4.446(3) | 4.446(3) | 4.4466(29) |
| - | $(4^+)$ | 4.8057(25) | 4.806[a] | 4.806[a] | 4.805[a] | 4.810(30) | 4.821(13) | 4.806(2) | 4.806(2) | 4.8061(16) |
| - | $(0^+)$ | 4.8270(25) | - | - | - | - | - | - | - | 4.8270(25) |
| $2^+$ | $2^+$ | 5.1415(17)[e] | 5.145(4) | 5.140(10) | 5.145(2) | - | - | - | - | 5.1431(12) |
| - | - | - | - | - | - | - | 5.229(12) | - | 5.229(12) | 5.229(12) |
| $4^+$ | $4^+$ | 5.286(6) | 5.291(4) | 5.291 | 5.291(3) | 5.310(30) | - | - | 5.330(20) | 5.2903(22) |
| $4^+$ | $4^+$ | 5.5116(25) | 5.515(4) | 5.526(8) | 5.515(5) | - | 5.562(28) | - | 5.562(28) | 5.5139(19) |

* Used in the present calibration.

[a] Used for calibration in the previous articles.

[b] Adopted $J^\pi$ values by Ref. [29].

[c] Mirror assignments, Fig. 6.3.

[d] Weighted average, only data given by Endt [46] are excluded.

[e] Averaged from the spectra at magnetic-field settings B1 and B2 at spectrometer angle $-0.3°$.

**4.1366(28) MeV $2^+$, 4.186(4) MeV $3^+$**: Our measured excitation energies for this doublet are in agreement with all experiments where this doublet is resolved, see Refs. [29, 73, 74].

**4.8057(25) MeV ($4^+$), 4.8270(25) MeV ($0^+$):** An indication that a doublet exists at around 4.8 MeV was given by Bohne *et al.* [72], Iliadis *et al.* [26], Caggiano *et al.* [28] and Bardayan *et al.* [27]. In the present experiment where a high resolution of 13 keV FWHM was achieved this doublet was resolved into levels at energies 4.8057(25) MeV and 4.8270(25) MeV. These two levels can be observed clearly in the spectrum obtained at a spectrometer angle of $-0.3°$; see Fig. 6.2. The level with the lower excitation energy of 4.8057(25) MeV can very well correspond to the level measured by Bell *et al.* [74] at 4.806(2) MeV. Possible $0^+$, $2^+$, and $4^+$ spin-parity values were correlated with this doublet in earlier articles [26, 27, 28, 72]. In the mirror spin-parity assignments given in Fig. 6.3 we suggest spin-parity $4^+$ and $0^+$ for the 4.8057(25) MeV and 4.8270(25) MeV levels, respectively.

**5.1415(17) MeV $2^+$, 5.5116(25) MeV $4^+$:** In Section 4.6 we already emphasized that we will not use these two levels for the calibration of our $^{26}$Si spectra. This was done in order to determine their excitation energies independently, considering the fact that there is a doublet around 4.8 MeV which was treated as a single level in previous experiments; see Refs. [27, 28, 29]. Our values are slightly lower, but still in agreement with the previous results. The presently adopted excitation energy of the second level is 5.5139(19) MeV, which overlaps with the $^{26}$Si proton-emission threshold 5.5123(1) MeV, calculated using the $^{26}$Si mass given by Parikh *et al.* [49].

The $^{26}$Si level measured at an excitation energy of 5.229(12) MeV in the (p,t) experiment by Paddock [73] is not observed in any other experiment, including the present (p,t) experiment and that by Bardayan *et al.* [27]. If the $^{26}$Mg $1^+$ state at 5.691 MeV corresponds to the $^{26}$Si $1^+$ level at an excitation energy of 5.672(4) MeV, as suggested in Fig. 6.3, then there is no corresponding $^{26}$Mg mirror level to the $^{26}$Si 5.229(12) MeV state. Consequently, the observed level at 5.229(12) MeV in Ref. [73] can be an overlap of the 5.1415(17) MeV and 5.286(6) MeV levels and the $^{10}C_{g.s.}$ impurity at the same position, which could not be resolved by Paddock [73].

The excitation energy of the state at 5.286(6) MeV has been determined from the spectrum measured at a spectrometer angle of $8°$, because this level was affected by an $^{14}$O contaminant line at $-0.3°$ spectrometer angle; see Fig. 6.2. In spite of the higher statistics at a spectrometer angle of $17°$, we used the result at a spectrometer angle of $8°$ because at this angle the systematic error is smaller than at a spectrometer angle of $17°$.

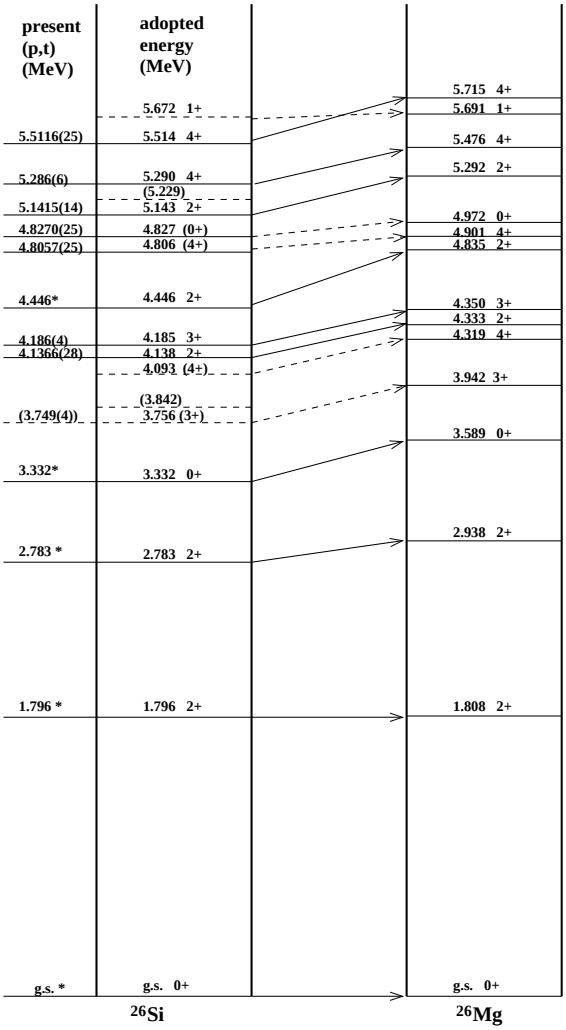


**Figure 6.3**: *Possible $^{26}$Si mirror assignments for levels below the proton-emission threshold. The $^{26}$Mg spin-parity values without brackets are taken from previous experiments Ref. [61]. The $^{26}$Si spin-parity values within brackets are possible mirror assignments. The full (dashed) arrows lines indicate definite (tentative) mirror assignments. The $^{26}$Mg spin-parity values are from Ref. [61]. See further Fig. 5.3 for more details.*

## 6.3 Region above the proton-emission threshold (5.5123 MeV - 9.164 MeV)

In this section we will discuss $^{26}$Si levels above the proton-emission threshold of 5.5123 MeV. The spectrum taken at the spectrometer angle of $-0.3^{\circ}$ using the 0.70 mg/cm$^2$ thick

$^{28}$Si target is presented in the upper panel of Fig. 6.4. To identify the $^{10}$C and $^{14}$O contaminant levels, we show in the bottom panel of Fig. 6.4 a spectrum taken at the same angle using a 1.00 mg/cm$^2$ thick Mylar target.

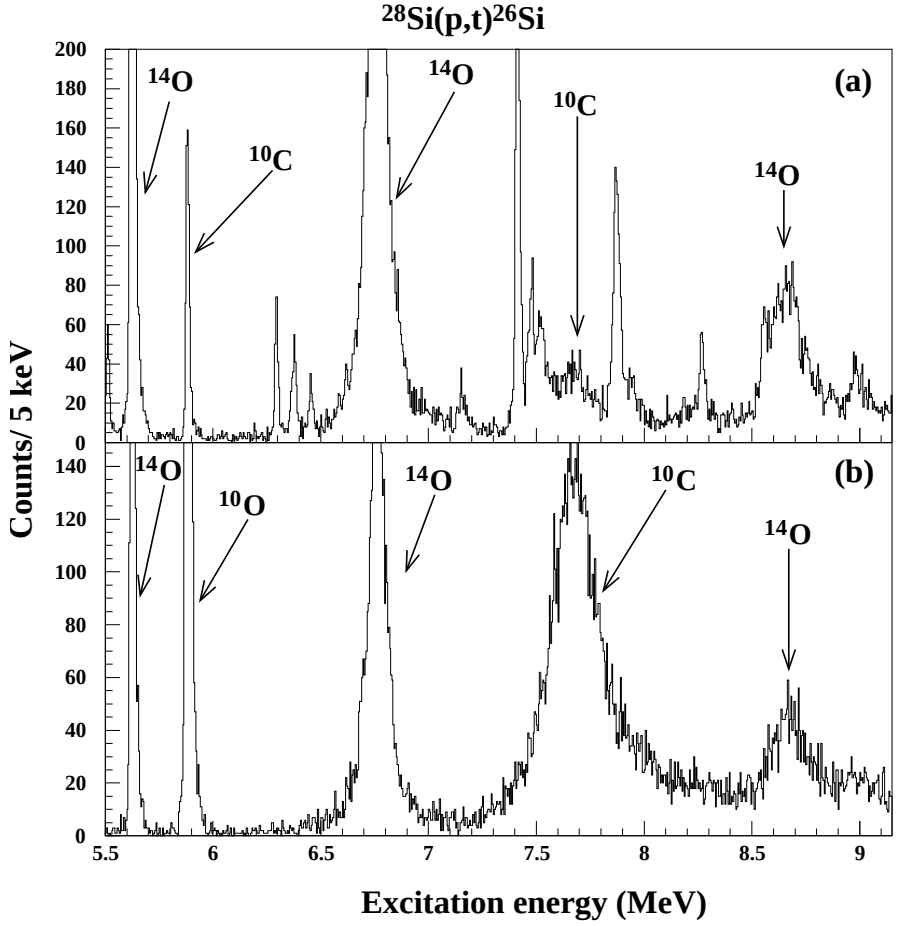


**Figure 6.4**: *(a) The spectrum taken using a 0.70 mg/cm$^2$ thick $^{28}$Si target at the spectrometer angle of $-0.3^\circ$. (b) The spectrum taken using a 1.00 mg/cm$^2$ thick Mylar target at the same spectrometer angle. The $^{10}$C and $^{14}$O impurity lines are indicated.*

The 0.7 mg/cm$^2$ thick $^{28}$Si target [1] consisted of three thin layers. In addition, we collected also spectra using a 1.86 mg/cm$^2$ thick natural Si target at all three spectrometer angles. By comparing differential cross sections for the $^{26}$Si levels measured at different time intervals on both Si targets (enriched and natural) we concluded that one layer was

[1] This target was made by Greene and Berg [75].

burned at the beginning of the measurements and one more later on. These burned layers decreased the amount of collected data and this can be seen in the $^{26}$Si spectra after subtraction of the $^{10}$C and $^{14}$O contaminants; see Fig. 6.5. The achieved statistics is much lower than achieved for the $^{24}$Mg target discussed in Chapter 4.

The burning of the Si target layers introduced a problem for the subtraction of contaminant lines from the $^{26}$Si spectra. The spectra obtained with the three-times thicker Mylar target have a resolution which is worse as compared to that of the $^{26}$Si spectra. This prevented us from obtaining a high quality subtracted spectra like the $^{22}$Mg spectra shown in Fig. 4.4. In Fig. 6.5, the remaining parts of the most prominent contaminant lines are indicated with "**B**". Because of these problems we accepted in our analysis only strongly populated $^{26}$Si levels or levels which are clearly visible in at least two spectra. In Fig. 6.5, the $^{26}$Si levels between the proton-emission threshold and $\alpha$-emission threshold are indicated by their excitation energy in the spectrum where their energies were determined.

The determined $^{26}$Si excitation energies for levels between the proton-emission and $\alpha$-emission thresholds are listed in column 3 of Table 6.2. Previous experimental results in this region are listed in columns 4 - 9 of Table 6.2. The presently adopted $^{26}$Si excitation energies are listed in the last column of Table 6.2. These have been obtained as weighted averages of all existing data listed in columns 3 to 8. Only data listed by Endt were not taken in the averages because they are averages of earlier existing data. In Table 6.1, we showed that our results are consistent with those from the previous experiments for levels below the proton-emission threshold. However, for the $^{26}$Si levels above the proton-emission threshold our results differ from results given by Parpottas *et al.* [29] and from some of the levels given by Bardayan *et al.* [27]; see columns 3, 4, and 6 of Table 6.2. As already discussed in section 6.2, the differences result from the use of the doublet at 4.806 MeV for the last calibration point in Refs. [27, 29]. However, our data are consistent with data given by Bohne *et al.* [72] and Paddock [73].

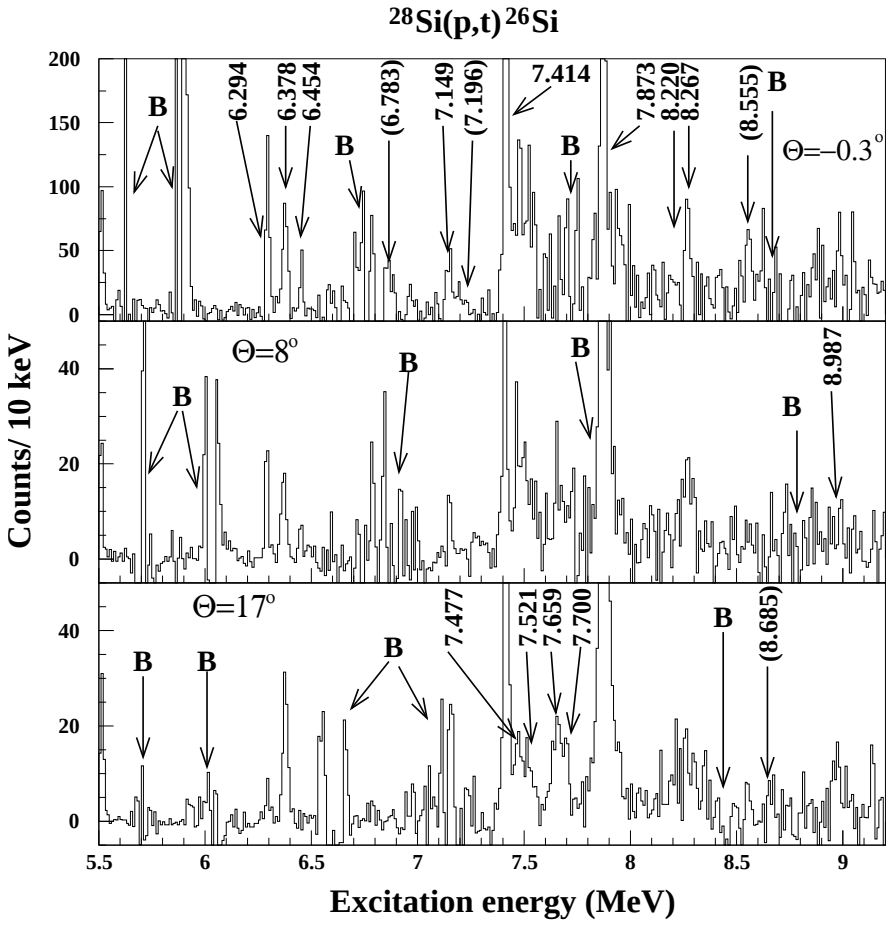


**Figure 6.5**: *The $^{28}$Si(p,t)$^{26}$Si spectra between the proton-emission threshold and the $\alpha$-emission threshold taken at the spectrometer angles $-0.3^{\circ}$, $8^{\circ}$, and $17^{\circ}$. The excitation energies of the analyzed $^{26}$Si levels are marked in the spectrum where they were determined. The remaining parts of the subtraction of $^{10}$C and $^{14}$O contaminant lines are indicated by "**B**". The determined excitation energies for $^{26}$Si are listed in the third column of Table 6.2. See further Fig. 4.5 for more details.*

**Table 6.2**: *Region above the proton-emission threshold (5.5123 - 9.164 MeV).*

| $J^\pi$ adopted[a] | $J^\pi$ mirror[b] | Present (p,t) | Ref. [29] ($^3$He,n) | Ref. [28] ($^3$He,$^6$He) | Ref. [27] (p,t) | Ref. [72] ($^3$He,n) | Ref. [73] (p,t) | Ref. [46] compilation | adopted present[c] |
|---|---|---|---|---|---|---|---|---|---|
| $4^+$ | $4^+$ | 5.5116(25) | 5.515(4) | 5.526(8) | 5.515(5) | - | 5.562(28) | 5.562(28) | 5.5139(19) |
| $1^+$ | $1^+$ | - | 5.670(4) | 5.678(8) | - | - | - | - | 5.672(4) |
| $0^+$ [d] | $0^+$ | (5.919(12))[e] | 5.912(4) | - | 5.916(2) | 5.910(30) | - | - | 5.9152(18) |
| $0^+$ | $3^+$ | (5.942(20))[e] | 5.946(4) | 5.945(8) | - | - | 5.960(22) | 5.940(25) | 5.946(4) |
| $2^+$ | $2^+$ | 6.2940(24) | 6.312(4) | - | 6.300(4) | 6.320(30) | - | - | 6.2991(18) |
| $2^+$ | $(4^+)$ | 6.3778(29) | 6.388(4) | - | 6.380(4) | - | 6.381(20) | 6.350(25) | 6.3810(20) |
| $0^+$ | $0^+$ | 6.4546(28) | 6.471(4) | - | - | 6.470(30) | - | 6.470(30) | 6.4600(23) |
| $3^-$ | $3^-$ | 6.783(5) | 6.788(4) | - | 6.787(4) | 6.780(30) | 6.786(29) | 6.789(17) | 6.7861(23) |
| - | $(5^+)$ | - | - | - | - | 6.880(30) | - | 6.880(30) | 6.88(3) |
| - | $(3^+)$ | - | - | - | 7.019(10) | - | - | - | 7.019(10) |
| $2^+$ | $2^+$ | 7.149(5) | 7.152(4) | - | 7.160(10) | 7.150(30) | 7.150(15) | 7.150(13) | 7.1514(28) |
| - | $(5^+)$ | (7.196(8)) | - | - | - | - | - | - | (7.196(8)) |
| $0^+$ | $0^+$ | 7.4135(23) | 7.425(4) | - | 7.425(7) | 7.390(30) | - | 7.390(30) | 7.4169(19) |
| $2^+$ | $2^+$ | 7.477(12) | 7.493(4) | - | 7.498(4) | 7.480(30) | 7.476(20) | 7.489(15) | 7.4941(27) |
| - | $(5^-)$ | 7.521(12) | - | - | - | - | - | - | 7.521(12) |
| - | $(2^+)$ | 7.659(12) | - | - | - | - | - | - | 7.659(13) |
| $3^-$ | $3^-$ | 7.700(12) | 7.694(4) | - | 7.687(22) | - | 7.695(30) | 7.695(30) | 7.694(4) |
| $1^-$ | $1^-$ | 7.873(4) | 7.899(4) | - | 7.900(22) | 7.900(30) | 7.902(21) | 7.892(15) | 7.8829(24) |
| - | $(3^+)$ | - | - | - | - | 8.120(30) | - | 8.120(20) | 8.12(3) |
|  | $(1^-)$ | 8.220(5) | - | - | - | - | - | - | 8.220(5) |
| - | $(2^+)$ | 8.267(4) | - | - | - | - | - | - | 8.267(4) |
| - | $(2^+)$ | (8.555(4)) | - | - | - | - | - | - | (8.555(4)) |
| - | $(4^+)$ | (8.685(12)) | - | - | - | 8.700(30) | - | - | 8.687(11) |
| - | $(4^+)$ | 8.987(7) | - | - | - | - | - | - | 8.987(7) |

[a] Adopted $J^\pi$ values by Ref. [29]. [b] Mirror assignments; see Fig. 6.6. [c] Weighted average, only data given by Endt [46] are excluded; see text. [d] Adopted from Ref. [27], in Ref. [29] a $3^+$ spin-parity was suggested. [e] Tentative excitation energies from the measurement at the spectrometer angle of 17°. These are not taken in the averaging process.

In the following we will discuss some of the levels individually.

**5.672(4) MeV $1^+$** (last column of Table 6.2): This level is assigned $1^+$ spin-parity in Refs. [28, 29]. This level is not observed in the present experiment, nor in previous (p,t) experiments [27, 73]. Because of this we assumed an unnatural $1^+$ spin-parity for this level in our spin-parity mirror assignments (Fig. 6.6), which is consistent with Refs. [28, 29].

**(5.919(12)) MeV $0^+$, (5.942(20)) MeV $3^+$:** These levels are observed in previous experiments [27, 29, 72]. The level at 5.919(12) MeV was assigned $0^+$ spin-parity from the DWBA analysis in Ref. [27] and the level at 5.942(20) MeV was assigned spin-parity $3^+$ from mirror assignments by us and Caggiano *et al.* [28]. In the present experiment we were not able to observe these two levels at $-0.3^\circ$ because of a $^{10}$C impurity line. At a spectrometer angle of $8^\circ$ they were not observed at all, and at $17^\circ$ the statistics did not allow us to make any conclusive decision.

**6.2940(24) MeV $2^+$, 6.3778(29) MeV ($4^+$), 6.4546(28) MeV $0^+$:** These three levels are clearly observed at $-0.3^\circ$ and $8^\circ$ spectrometer angles. Their deduced excitation energies are in agreement with Refs. [27, 72, 73] but not with Ref. [29]. This discrepancy might be attributed to the use of the 4.806 MeV doublet for the calibrations performed by Ref. [29]. In our present mirror spin-parity assignments we were not able to follow the spin-parity assignments given by Parpottas *et al.* [29]. Because the spin-parity assignment for these three levels in Refs. [27, 72] were based on a DWBA analysis we adopted a $2^+$ spin-parity assignment for the level at 6.2940(24) MeV. In addition we assigned a ($4^+$) spin-parity to the level at 6.3778(29) MeV; see Fig. 6.6.

**7.521(12) MeV ($5^-$), 7.659(12) MeV ($2^+$):** We resolved these two, previously not observed, states. The 12 keV error is caused by the larger uncertainty in the determination of $E_x$ at the $17^\circ$ spectrometer angle, which is related to kinematic broadening. These two levels are not clearly observed at $-0.3^\circ$ and $8^\circ$ spectrometer angles because at those angles they are covered by a broad $^{10}$C resonance; see Fig. 6.4.

**8.220(5) MeV ($1^-$), 8.267(4) MeV ($2^+$), 8.987(7) MeV ($4^+$):** These three resolved levels are observed at all three spectrometer angles. Their possible mirror spin-parity assignments can be seen in Fig. 6.6.

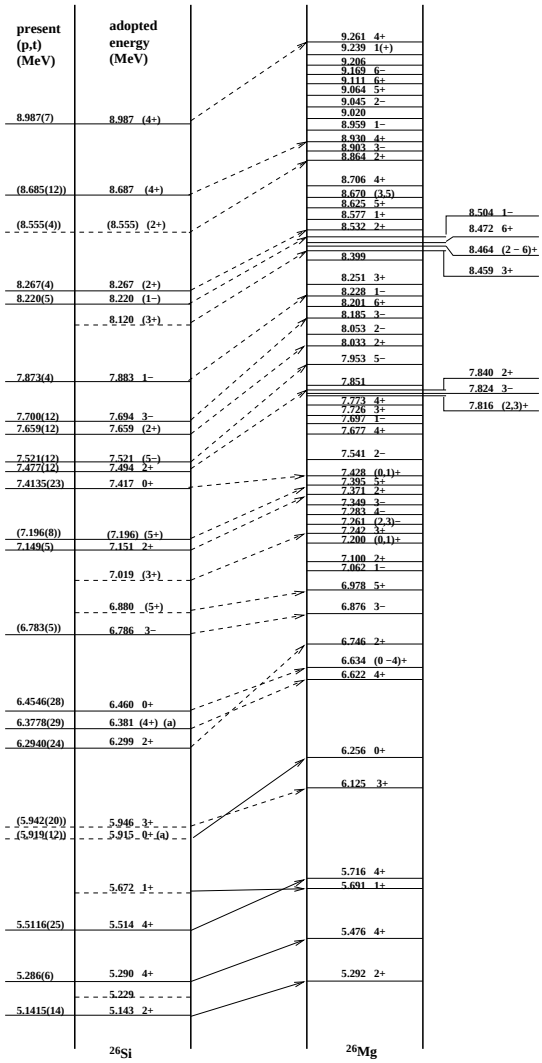


**Figure 6.6**: *The possible $^{26}$Si mirror assignments for levels above the proton-emission threshold. The $^{26}$Si spin-parity assignments without brackets are taken from previous experiments [61]. The $^{26}$Si spin-parity values within brackets are possible mirror assignments. The full (dashed) arrows indicate definite (tentative) mirror assignments. The $^{22}$Ne spin-parity values are from Ref. [61]. The $^{26}$Si adopted energies are taken from the last column of Table 6.2. These spin-parity assignments will be used for reaction-rate calculations. (a) From DWBA analysis in Ref. [27]. See further Fig. 5.3 for more details.*

## 6.4 Region above the $\alpha$-emission threshold (9.164 MeV)

The $^{26}$Si levels above the $\alpha$-emission threshold are important for the $^{22}$Mg($\alpha$,p)$^{25}$Al reaction in X-ray bursts and supernovae; see Section 2.5. In the present experiment we identified four $^{26}$Si levels above the $\alpha$-emission threshold and for three more levels tentative excitation energies were determined. All these levels are listed in Table 6.3 and shown in Fig. 6.7. Possible mirror assignments are given in column 1 of Table 6.3.

The tentative levels above 10.0 MeV are listed because they could be identified at two spectrometer angles at a consistent excitation energy. Because of low statistics and a strong influence of the $^{10}$C and $^{14}$O impurity lines, we have not been able to unambiguously identify levels above 10 MeV excitation energy in $^{26}$Si. Large errors due to the subtraction of impurity lines are present. We also fitted the area betwen 10 and 12 MeV with a constant straight line and obtained a reduced chi-square of around unity. Consequently, all listed possible levels above 10 MeV excitation energy can be simply statistical fluctuations.

**Table 6.3**: *Region above the $\alpha$-emission threshold (9.164 MeV) in $^{26}$Si.*

| $J^\pi$ mirror | $E_x$ $^{26}$Si (MeV) | $E_x$ $^{26}$Mg (MeV) |
|---|---|---|
| $(4^+)$ | 9.314(6) | 9.579(3) |
| $(2^+)$ | 9.604(13) | 9.85652(6) |
| $(5^-)$ | 9.760(4) | 10.040(2) |
| $(0^+)$ | 9.9017(25) | 10.159(3) |
| - | (10.434(13)) | - |
| - | (10.65(6)) | - |
| - | (11.01(4)) | - |

There are many more observed levels in $^{26}$Mg for this excitation-energy range as compared to $^{26}$Si, and there is no clear marking point for mirror assignments. Because of this a mirror energy difference between 250 keV and 350 keV was maintained as for levels at excitation energy higher than 7.5 MeV as shown in Fig. 6.6. Because the (p,t) reaction preferably excites natural-parity states, we correlated observed $^{26}$Si levels with known natural-parity states in $^{26}$Mg. In this way, we obtained mirror assignments as presented in Table 6.3.

## 6.5 Astrophysical implications for the $^{25}$Al(p,$\gamma$)$^{26}$Si reaction

The $^{26}$Si levels relevant for the $^{25}$Al(p,$\gamma$)$^{26}$Si reaction have been studied in recent experiments [26, 27, 28, 29]. The difference between the excitation energies measured in the

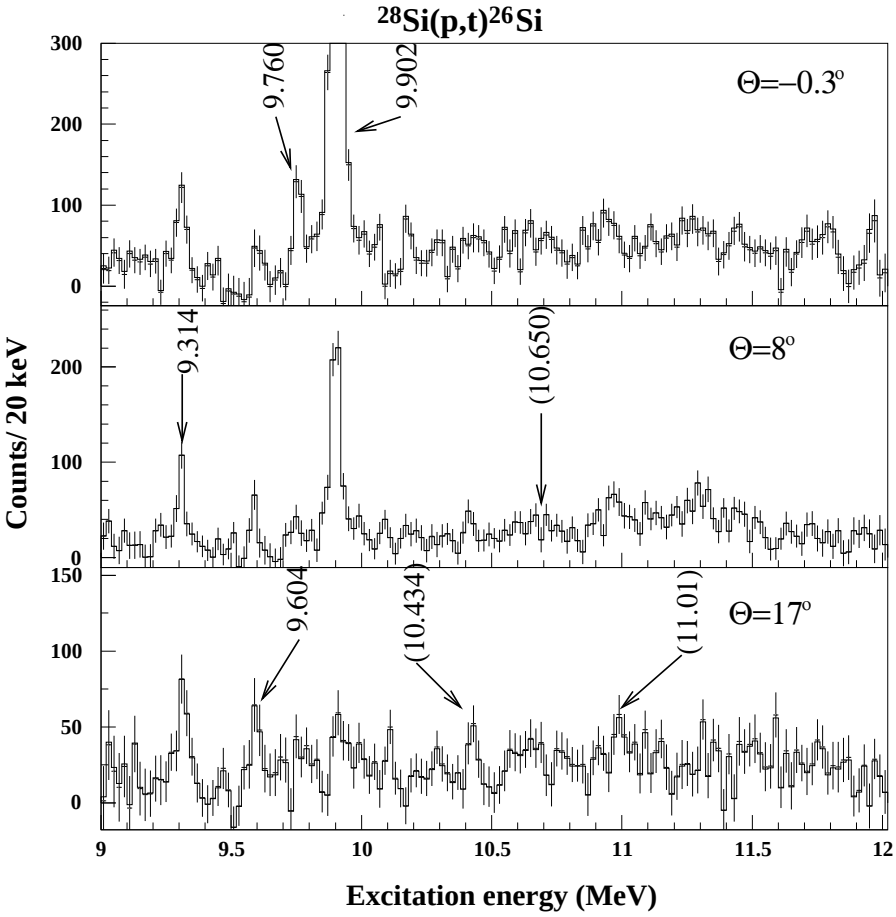


**Figure 6.7**: *The $^{28}$Si(p,t)$^{26}$Si spectra above the $\alpha$-emission threshold measured at $-0.3^\circ$, $8^\circ$, and $17^\circ$ spectrometer angles. The energy determined for each peak is marked in the spectrum used to determine it. The determined excitation energies for $^{26}$Si are listed in the second column of Table 6.3. See further Fig. 4.5 for more details.*

present experiment and those in Ref. [29] for levels above the proton-emission threshold has already been discussed in Section 6.3. For the discussion of the $^{25}$Al(p,$\gamma$)$^{26}$Si and $^{22}$Mg($\alpha$,p)$^{25}$Al reaction rates we will use only adopted excitation energies listed in the last columns of Table 6.2 and Table 6.3, respectively.

From Refs. [26, 27, 28, 29] it can bee seen that the resonances at 0.159(4) MeV ($1^+$), 0.4029(18) MeV ($0^+$), and 0.434(4) MeV ($3^+$) dominate the $^{25}$Al(p,$\gamma$)$^{26}$Si reaction rates for all astrophysically relevant temperatures. In the present experiment we did not observe

any of these three levels, including the natural-parity $0^+$ level. Taking into account possible errors introduced in previous experiments by using the doublet at 4.806 MeV for the calibration of the excitation energy, a new measurement of the excitation energies for these three levels will be valuable.

On basis of the adopted $^{26}$Si excitation energies, listed in the last column of Table 6.2, we have calculated the $^{25}$Al(p,$\gamma$)$^{26}$Si reaction rates. The important difference between the present calculations and those done previously [28, 29] is a new value for the proton-emission threshold for $^{26}$Si. Instead of the value previously used (5.518 MeV), the new $^{26}$Si proton-emission threshold value is 5.5123(10) MeV; see the conclusion in Section 4.6.

As a consequence the 5.5139(19) MeV level is actually above the $^{26}$Si proton-emission threshold. However, its 0.0016 MeV resonance energy is well below the Gamow window for the $^{25}$Al(p,$\gamma$)$^{26}$Si reaction for temperatures above 0.01 $T_9$. Therefore, we will not use this level in our reaction-rate calculations.

For temperatures between 0.01 $T_9$ and 1.5 $T_9$ the contribution of the direct reaction rate in the $^{25}$Al(p,$\gamma$)$^{26}$Si reaction is taken from Ref. [26].

Since there is no direct measurement of $^{26}$Si resonance strengths we rely on the calculations using Eq. 2.28. The first few $^{26}$Si levels above the proton-emission threshold are well below the Coulomb barrier and, consequently, $\Gamma_p \ll \Gamma_\gamma$ and $\omega_\gamma \approx \omega\Gamma_p$. The proton partial decay width is calculated using the recipe outlined in Ref. [70]:

$$\Gamma_p = \frac{3\hbar^2}{\mu R_n^2} P_l \Theta_{sp}^2 C^2 S \tag{6.1}$$

where $\Theta_{sp}^2$ is the dimensionless single-particle reduced width, and the rest of the parameters are the same as for Eq. 2.29. In order to be consistent with the formalism given in Chapter 2, the $\Theta_{sp}^2$ is given by:

$$\Theta_{sp}^2 = \frac{R_n}{3}\phi_l^2(R_n) \tag{6.2}$$

and not as given in Ref. [70]:

$$\Theta_{sp}^2 = \frac{R_n}{2}\phi_l^2. \tag{6.3}$$

Therefore, in order to use the $\Theta_{sp}^2$ values calculated according to Iliadis [70] we will scale them with a factor $\frac{2}{3}$. The $\phi_l^2(R_n)$ denotes the square of the single-particle radial wave function of the $l$ orbit at the interaction radius $R_n$ given by Eq. 2.9. In the literature the single-particle reduced widths are often set equal to unity. As shown by Iliadis [70] this approach can produce a significant error in the $\Gamma_p$ calculations. Iliadis investigated the systematic dependence of $\Theta_{sp}^2$ on variations in bombarding energy, target mass, charge, interaction radius, and radial and angular quantum numbers. We calculated the proton partial reduced widths for the $^{26}$Si resonances by using the formalism given in Ref. [70].

In Table 6.4 we list levels in $^{26}$Si above the proton-emission threshold with their proton and gamma partial decay widths. The proton partial decay widths marked with superscript $^{a}$ in Table 6.4 are calculated on basis of the $^{26}$Mg single-particle spectroscopic factors taken from Ref. [69]. The theoretically calculated single-particle spectroscopic factor taken from Ref. [26] is marked with superscript $^{b}$ in Table 6.4. The single-particle reduced widths $\Theta^2_{sp}$ are calculated on basis of data given by Iliadis [70]. The penetrability of the Coulomb and centrifugal barrier was calculated using the PENE code [35].

In order to calculate $\Gamma_\gamma$, we used the measured half-life data for decay via $\gamma$-emission [61] of corresponding levels in the mirror nucleus $^{26}$Mg. As for the case of the $^{22}$Mg data (Section 5.8) we corrected in the same way these values for the difference in $\gamma$-ray transition energies of mirror transitions; those levels are marked by the superscript $^{c}$ in Table 6.4.

**Table 6.4**: *The $^{25}$Al(p,$\gamma$)$^{26}$Si reaction: resonance energies, spin assignments and resonance strengths.*

| $E_x$ $^{f}$ (MeV) | $E_{res}$ (MeV) | $J^\pi$ mirror | $\Gamma_p$ (eV) | $\Gamma_\gamma$ mirror (eV) | $\omega\gamma$ (eV) |
|---|---|---|---|---|---|
| 5.6716 | 0.1593 | $1^+$ | 4.22E-8 $^{a}$ | 1.10E-1 $^{e}$ | 1.06E-8 |
| 5.9152 | 0.4029 | $0^+$ | 1.05E-2 $^{b}$ | 8.03E-3 $^{c}$ | 3.79E-4 |
| 5.9462 | 0.4339 | $3^+$ | 7.93E-1 $^{a}$ | 4.58E-2 $^{c}$ | 2.53E-2 |
| 6.2991 | 0.7868 | $2^+$ | 3.50E+0 $^{a}$ | 2.65E-2 $^{c}$ | 1.10E-2 |
| 6.3810 | 0.8687 | $(4^+)$ | 1.51E+0 $^{b}$ | 2.65E-2 $^{c}$ | 1.96E-2 |
| 6.4600 | 0.9477 | $0^+$ | - | 9.04E-2 $^{c}$ | 7.54E-3 |
| 6.7861 | 1.2738 | $3^-$ | 7.70E+2 $^{a}$ | 7.66E-3 $^{c}$ | 4.47E-3 |
| 6.8800 | 1.3677 | $(5^+)$ | 1.28E+2 $^{a}$ | 5.39E-2 $^{c}$ | 4.94E-2 |
| 7.0190 | 1.5067 | $(3^+)$ | 2.64E+3 $^{a}$ | 9.32E-2 $^{c}$ | 5.44E-2 |
| 7.1514 | 1.6391 | $2^+$ | - | 1.00E-2 $^{d}$ | 4.17E-3 |
| 7.1955 | 1.6832 | $(5^+)$ | 9.23E+2 $^{a}$ | 4.53E-2 $^{c}$ | 4.15E-2 |
| 7.4169 | 1.9046 | $0^+$ | - | 1.00E-2 $^{d}$ | 8.33E-4 |
| 7.4941 | 1.9818 | $2^+$ | - | 1.00E-2 $^{d}$ | 4.17E-3 |
| 7.5205 | 2.0082 | $(5^-)$ | - | 3.26E-2 $^{c}$ | 2.99E-2 |
| 7.6592 | 2.1469 | $(2^+)$ | - | 1.00E-2 $^{d}$ | 4.17E-3 |
| 7.6944 | 2.1821 | $3^-$ | - | 1.00E-2 $^{d}$ | 5.83E-3 |
| 7.8829 | 2.3706 | $1^-$ | - | 5.17E-1 $^{c}$ | 1.29E-1 |
| 8.1200 | 2.6077 | $(3^+)$ | 1.91E+4 $^{a}$ | 1.00E-2 $^{d}$ | 5.83E-3 |

$^{a}$ Particle decay widths calculated using the single-particle spectroscopic factors from the mirror nucleus $^{26}$Mg, Ref. [69].
$^{b}$ Theoretically calculated single-particle spectroscopic factor taken from Ref. [26].
$^{c}$ $\Gamma_\gamma$ values calculated from the half-life data for $^{26}$Mg mirror levels [61].
$^{d}$ A constant value of 0.01 eV is assumed for $\Gamma_\gamma$.
$^{e}$ Theoretically calculated $\Gamma_\gamma$ value, taken from Ref. [26].
$^{f}$ $^{26}$Si excitation energies are taken from last column in Table 6.2.
$J^\pi$ values without brackets are taken from Ref. [29].
$J^\pi$ values within brackets are obtained by the mirror assignments given in Fig. 6.6.

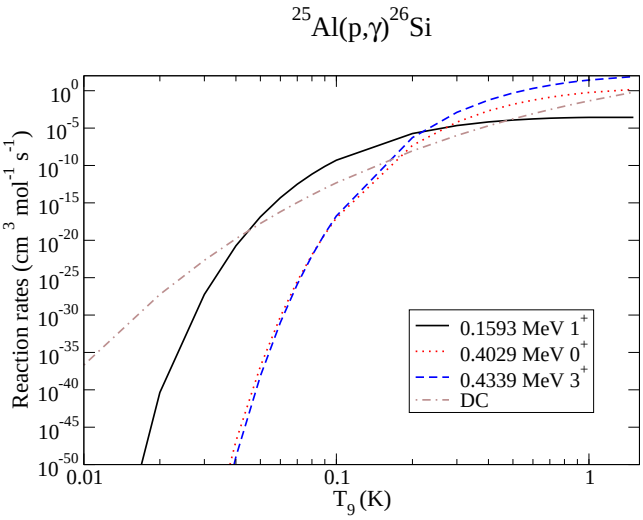


**Figure 6.8**: *The contributions of the first three resonances above the proton-emission threshold to the $^{25}$Al(p,$\gamma$)$^{26}$Si reaction rates. The direct capture rates are taken from Ref. [26].*

For levels indicated by the superscript $^d$ we adopted a constant $\Gamma_\gamma$ value of 0.01 eV, because there are no experimental or theoretical data for those levels. For the 0.159 MeV $1^+$ resonance the theoretically calculated [69] $\Gamma_\gamma$ value is used, since the experimental value has only a lower limit [61] of 0.08 eV.

For those levels for which the $\Gamma_\gamma$ and $\Gamma_p$ values are known we calculated the resonance strength using the exact formula given in Eq. 2.28. For those levels for which there is no information on $\Gamma_p$, we used Eq. 5.3, since for all levels above 5.9462 MeV $\Gamma_p \gg \Gamma_\gamma$.

On basis of the data presented in Table 6.4, we have computed new $^{25}$Al(p,$\gamma$)$^{26}$Si reaction rates. The contributions from the first three resonances and direct capture are presented in Fig. 6.8. The resonant reactions dominate for temperatures beyond 0.04 $T_9$.

As can be seen from Fig. 6.8, the resonance reaction rates are completely dominated by the two unnatural parity resonances (0.159 MeV $1^+$ and 0.434 MeV $3^+$). This is in contradiction with the results shown in Ref. [29] where the 0.4029 MeV resonance dominates for stellar temperatures above 1 $T_9$.

In Fig. 6.9 we show the total $^{25}$Al(p,$\gamma$)$^{26}$Si reaction rates in comparison with those computed by Caggiano *et al.* [28] and Parpottas *et al.* [29]. The main difference between the present calculations and those listed in Refs. [28, 29] is in the temperature range from 0.04 $T_9$ up to 0.2 $T_9$. This difference is due to using different values for the single-particle spectroscopic factors. In the present calculations the single-particle spectroscopic factors have been taken from Ref. [69] and in the previous calculations they are taken from Il-

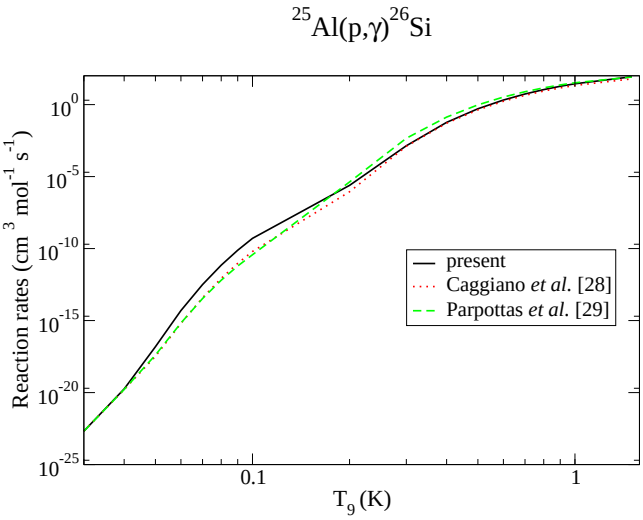


**Figure 6.9**: *The $^{25}$Al(p,$\gamma$)$^{26}$Si reaction rates as function of temperature. The dotted and dashed curves indicate reaction rates calculated in Refs. [28, 29], respectively.*

iadis *et al.* [26]. At stellar temperatures above 0.2 $T_9$ all calculated reaction rates are in agreement.

## 6.6 Astrophysical implications for the $^{22}$Mg($\alpha$,p)$^{25}$Al reaction

In Section 1.4 we mentioned that the $^{26}$Si levels above the $\alpha$-emission threshold are important for the bolometrically double-peaked type I X-ray bursts. $^{22}$Mg is a $\beta^+$-unstable nucleus which has a low $Q$-value for the $^{22}$Mg(p,$\gamma$)$^{23}$Al reaction. Consequently, photodisintegration of $^{23}$Al prevents a significant flow through a subsequent $^{23}$Al(p,$\gamma$) reaction. However, this waiting point can be bridged by the $^{22}$Mg($\alpha$,p)$^{25}$Al reaction. From Section 6.4 we know that there are no published experimental data for the relevant region in $^{26}$Si. Since we could not make spin assignments for the states identified in the present experiment we will rely on the mirror spin assignments given in Section. 6.4. The required alpha spectroscopic factors, which are used to perform the reaction-rate calculations are obtained from Ref. [71] for the $^{26}$Mg levels. The penetrability through the Coulomb and centrifugal barriers is calculated using the PENE code [35]. The obtained $S_\alpha$ values for $^{26}$Mg are listed in Table 6.5.

**Table 6.5**: *The $S_\alpha$ parameters for the $^{22}Ne(\alpha,n)^{25}Mg$ reaction taken from Ref. [71].*

| $E_x(^{26}Mg)$ (MeV) | $E_{res}$ (MeV) | $J^\pi$ | $S_\alpha$ |
|---|---|---|---|
| 10.693 | 0.078 | $4^+$ | 1.49E-2 |
| 10.945 | 0.330 | $2^+$, $3^-$ | 3.71E-2 |
| 11.112 | 0.497 | $2^+$ | 3.51E-3 |
| 11.153 | 0.538 | $1^-$ | 7.24E-3 |
| 11.163 | 0.548 | $2^+$ | 3.51E-3 |
| 11.171 | 0.556 | $2^+$ | 3.54E-3 |
| 11.183 | 0.568 | $1^-$ | 3.62E-3 |
| 11.194 | 0.579 | $2^+$ | 3.46E-3 |
| 11.274 | 0.659 | $2^+$ | 3.53E-3 |
| 11.286 | 0.671 | $1^-$ | 3.64E-3 |
| 11.310 | 0.695 | $1^-$ | 2.91E-2 |
| 11.326 | 0.711 | $1^-$ | 2.91E-2 |
| 11.328 | 0.713 | $1^-$ | 1.14E-1 |

**Table 6.6**: *The adopted $S_\alpha$ values for the relevant levels in $^{26}Si$.*

| $J^\pi$ | $S_\alpha$ |
|---|---|
| $0^+$ | 0.037 |
| $1^-$ | 0.007 |
| $2^+$ | 0.037 |
| $3^-$ | 0.007 |
| $4^+$ | 0.015 |
| $5^-$ | 0.007 |

From these $S_\alpha$ values we determined $S_\alpha$ values for $^{26}$Si. From Table 6.5 it can be seen that we have $S_\alpha$ values only for $1^-$, $2^+$, and $4^+$ natural-parity levels. For $0^+$ levels we will adopt the $S_\alpha$ value 3.7E-2 as for the $2^+$ state at 10.945 MeV. For $3^-$ and $5^-$ states we adopted the value 7E-3 as for the $1^-$ state at 11.153 MeV, because no other negative natural-parity $3^-$, $5^-$ states were observed for which we obtained an $S_\alpha$ value. We chose these particular values for $S_\alpha$ because we observed only a few $^{26}$Si levels just above the $\alpha$-emission threshold, and we chose to use these $S_\alpha$ values for the corresponding $^{26}$Mg mirror levels just above the $\alpha$-emission threshold. In Section 6.4 we mentioned that we will only use natural-parity states for the present mirror assignments. The adopted $S_\alpha$ values for $^{26}$Si are listed in Table 6.6.

We used the method of narrow resonances to calculate the $^{22}$Mg($\alpha$,p)$^{25}$Mg reaction rates; the parameters are listed in Table 6.7.

As in Section 5.7 we will perform additional calculations using random spin-parity assignments to investigate the estimated error which may originate from the chosen spin assignment. In this case we will limit the spin value to 5. The reason is that in our experiment we did not observe any known level with a spin value of 6 or higher. Furthermore,

**Table 6.7**: *The adopted $S_\alpha$ values for the $^{22}$Mg($\alpha$,p)$^{25}$Al reaction.*

| $E_x(^{26}Si)$ (MeV) | $E_r$ (MeV) | $J^\pi$ | $S_\alpha$ |
|---|---|---|---|
| 9.314 | 0.150 | $(4^+)$ | 1.5E-2 |
| 9.603 | 0.440 | $(2^+)$ | 3.7E-2 |
| 9.760 | 0.596 | $(5^-)$ | 7.0E-3 |
| 9.902 | 0.738 | $(0^+)$ | 3.7E-2 |

**Table 6.8**: *The spin values and resonance strengths for the four resonances in the $^{22}$Mg($\alpha$,p)$^{25}$Al reaction.*

| | mirror [a] | | RND1 [b] | | RND2 [b] | |
|---|---|---|---|---|---|---|
| $E_{res}$ (MeV) | J | $\omega\gamma$ (eV) | J | $\omega\gamma$ (eV) | J | $\omega\gamma$ (eV) |
| 0.150 | 4 | 1.00E-36 | 1 | 4.31E-35 | 4 | 1.00E-36 |
| 0.440 | 2 | 2.40E-14 | 1 | 9.41E-15 | 0 | 3.12E-14 |
| 0.596 | 5 | 1.27E-13 | 5 | 1.27E-13 | 2 | 2.01E-10 |
| 0.738 | 0 | 8.82E-08 | 0 | 8.82E-08 | 1 | 2.73E-08 |

[a] Spin and resonance strength for the mirror assignments given in Figs. 5.9 and 5.12.
[b] Spin and resonance strength for the randomly generated spins of states.

an equal probability for all possible spin-values is assumed. The results of the calculations are listed in Table 6.8 and shown in Fig. 6.10.

The obtained reaction rates differ by up to a factor of three, but it must be emphasized that the difference is small compared to calculations where either very small or very large spin values are used for all four levels. This is due to a large difference in the penetrability for different angular momenta. For example, the ratio between the resonance strengths for states with angular momenta $l$=0 and $l$=5 can be up to 1000. A conservative calculation would be if we use only the spin values 2 and 3, because these values are in between the smallest and largest possible values. With the assumption that the given $\alpha$-spectroscopic factors are correct and the correct mirror spin assignments have been used, then the calculated error only originates from the error in the excitation energy. The relative error in the reaction rate for the interval of stellar temperatures between 0.1 $T_9$ and 10 $T_9$ is below 17%.

From this discussion it can be concluded that the largest contribution to the uncertainty in the calculated rates is due to the unknown values for the spin and parity and not to the uncertainty in the deduced excitation energy. Furthermore, the uncertainty introduced by the spin-parity assignments is also larger than the uncertainty introduced by the $S_\alpha$ values used.

The contribution from all four resonances is shown in Fig. 6.11. The 0.440 MeV and

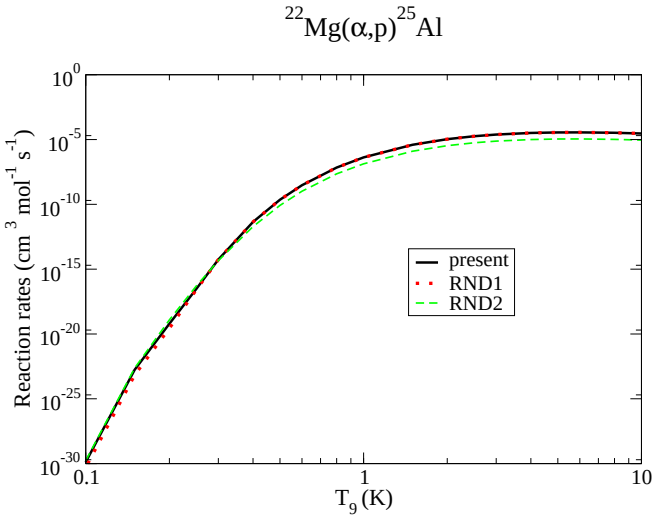


**Figure 6.10**: *The $^{22}$Mg($\alpha$,p)$^{25}$Al reaction rate as function of the temperature for the three different cases listed in Table 6.8.*

0.738 MeV resonances yield the dominant contribution for the entire interval of X-ray burst temperatures (0.1 - 10 $T_9$). The 0.150 MeV resonance is below the Gamow window for the $^{22}$Mg($\alpha$,p)$^{25}$Al reaction, and regardless of the choice for the spin value its contribution can not exceed the yield of the 0.440 MeV resonance. With the adopted spin value for the 0.738 MeV resonance, it completely dominates the reaction rate for temperature above 0.2 $T_9$. However, if the 0.596 MeV resonance has spin 0, this resonance will dominate for the temperature above 0.2 $T_9$.

From the previous discussion we conclude that for a more accurate reaction-rate calculation of the $^{22}$Mg($\alpha$,p)$^{25}$Al reaction it is necessary to obtain resonance strengths and spin information for $^{26}$Si levels above the $\alpha$-emission threshold. Since the $^{28}$Si(p,t)$^{26}$Si reaction preferably excites natural-parity states, it is necessary to perform experiments where also unnatural-parity states can be studied, e.g. $^{29}$Si($^{3}$He,$^{6}$He)$^{26}$Si. The large contribution of unnatural-parity states can be seen in Section 6.5, where we discussed the $^{25}$Al(p,$\gamma$)$^{26}$Si reaction rates.

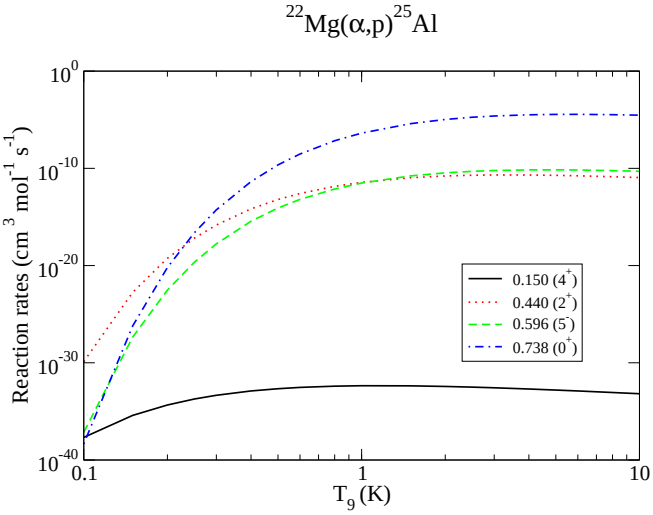


**Figure 6.11**: *The $^{22}$Mg($\alpha$,p)$^{25}$Al reaction rate as function of temperature with the separate contributions from all four resolved resonances. See further Fig. 4.5 for more details.*

## 6.7 Summary

In this chapter we discussed measured $^{26}$Si levels and their influence on the calculated rates for the $^{22}$Mg($\alpha$,p)$^{25}$Al and $^{25}$Al(p,$\gamma$)$^{26}$Si reactions. With an unprecedented resolution of 13 keV (FWHM) for the (p,t) experiment, we were able to resolve 38 levels in $^{26}$Si, 14 of which were observed for the first time. The errors in excitation energies for some of the measured levels decreased by 50%. This leads to a decrease in the relative error in the calculated reaction rate, which originates from the errors in the excitation energies of the resonances, to below 17%.

By measuring the levels at 4.8056(20) MeV and 4.8270(19) MeV we resolved a doublet at 4.806 MeV which was hitherto unresolved in previous $^{26}$Si experiments. The unresolved combined peak was until now used as a calibration point for the determination of the excitation energies of higher lying levels. In the present experiment we measured for the first time four levels above the $\alpha$-emission threshold.

Our calculated $^{25}$Al(p,$\gamma$)$^{26}$Si reaction rate is similar to those calculated in Refs. [28, 29]. This similarity can be attributed to the use of the same proton spectroscopic factors in all calculations as well as resonance energies which are not very much different. The main difference between the present calculations and those listed in Refs. [28, 29] is found in the temperature range from 0.04 $T_9$ up to 0.2 $T_9$. This difference is due to using different values for the single-particle spectroscopic factors. At stellar temperatures above 0.2 $T_9$ all calculated reaction rates are in agreement.

Our calculated reaction rate for the $^{22}$Mg($\alpha$,p)$^{25}$Al reaction is for the first time calculated on basis of the experimentally measured $^{26}$Si levels above the $\alpha$-emission threshold.